REPORT

PALEOCLIMATE

Cenozoic evolution of deep ocean temperature from clumped isotope thermometry

A. N. Meckler[1]*, P. F. Sexton[2], A. M. Piasecki[1]†, T. J. Leutert[1], J. Marquardt[1], M. Ziegler[3], T. Agterhuis[3], L. J. Lourens[3], J. W. B. Rae[4], J. Barnet[4], A. Tripati[5], S. M. Bernasconi[6]

Characterizing past climate states is crucial for understanding the future consequences of ongoing greenhouse gas emissions. Here, we revisit the benchmark time series for deep ocean temperature across the past 65 million years using clumped isotope thermometry. Our temperature estimates from the deep Atlantic Ocean are overall much warmer compared with oxygen isotope–based reconstructions, highlighting the likely influence of changes in deep ocean pH and/or seawater oxygen isotope composition on classical oxygen isotope records of the Cenozoic. In addition, our data reveal previously unrecognized large swings in deep ocean temperature during early Eocene acute greenhouse warmth. Our results call for a reassessment of the Cenozoic history of ocean temperatures to achieve a more accurate understanding of the nature of climatic responses to tectonic events and variable greenhouse forcing.

Throughout the Cenozoic era (the past 65 million years), Earth has experienced a large range of climate states (*1*, *2*), moving from greenhouse climates with high levels of atmospheric CO_2 and minimal ice on land to an icehouse world with large-scale, bipolar glaciation. Reconstructions of past temperatures offer unique insights into the response of the climate system to varying levels of CO_2 and other influences such as tectonically forced changes in ocean circulation. These reconstructions additionally serve as crucial benchmarks for assessing the performance of climate models (*3*). Deep ocean temperature is commonly used to obtain globally representative temperature estimates on million-year time scales [e.g., (*4, 5*)] because the deep ocean constitutes an extremely large and comparatively stable heat reservoir.

The key approach to reconstructing deep ocean temperatures, especially through the early Cenozoic, has been the analysis of the oxygen isotopic composition of shells of benthic foraminifera ($\delta^{18}O_b$) from deep ocean sediments. $\delta^{18}O_b$ reflects deep ocean temperature but also seawater isotopic composition ($\delta^{18}O_{sw}$) at the time of shell formation. The canonical view has been that before Antarctica was continually glaciated, $\delta^{18}O_{sw}$ had an assumed "ice-free Earth" value of −0.9 to −1.2‰ (*1*, *6*), and that temperature was the single most important influence on $\delta^{18}O_b$. Paleocene and early to middle Eocene temperatures are therefore typically calculated directly from $\delta^{18}O_b$ using established temperature calibrations [e.g., (*7*)]. This approach has yielded deep ocean temperatures of up to 12°C (*1*) to 14°C (*6*) during the warmest part of the Cenozoic, the early Eocene climatic optimum [EECO, 52 to 49 million years ago (Ma)]. However, the long-standing assumptions made as part of this established approach are largely uncorroborated (*6*, *8*). $\delta^{18}O_{sw}$ indeed reflects continental storage of ice, but also that of groundwater, and can in addition be related to changes in salinity and influenced by long-term changes in interactions between seawater and oceanic crust. Furthermore, nonthermal, physiological influences on $\delta^{18}O_b$ are not well understood (*7*) but are evident from $\delta^{18}O_b$ offsets between different species [e.g., (*9*)].

Additional proxy constraints have previously been sought from the Mg/Ca ratio of benthic foraminifera [e.g., (*10, 11*)], a temperature proxy that is independent of $\delta^{18}O_{sw}$. However, like $\delta^{18}O_b$, the Mg/Ca proxy suffers from nonthermal influences such as changes in seawater Mg/Ca ratio and carbonate chemistry (*12*) and physiological effects necessitating species-specific calibrations (*8*). Given these potential confounding influences on previous proxy records, the Cenozoic evolution of deep ocean temperature remains highly uncertain.

Here, we report the first Cenozoic record of deep ocean temperature based on carbonate clumped isotope (Δ_{47}) thermometry. The clumped isotope method takes advantage of the temperature dependence of isotopic ordering within molecules (*13*). It has the benefit that it does not require knowledge about seawater composition and is not measurably affected by physiological factors during the formation of foraminifera shells (see the supplementary materials and methods). Our record is predominantly from sites with exceptional foraminifera preservation in the North Atlantic, a region of major influence on global ocean circulation and climate. The reported clumped isotope temperatures each combine 13 to 45 replicate analyses of different foraminifera species. Species- or genus-specific $\delta^{18}O_b$ and carbon isotopic composition ($\delta^{13}C$) are obtained from the same measurements. The Δ_{47} temperatures show many similarities, but also marked differences, compared with previous reconstructions of deep ocean temperatures based on $\delta^{18}O_b$ (Fig. 1A and fig. S6). We observed the same overall trend across the Cenozoic, attesting to the fact that the large-scale features of the canonical $\delta^{18}O_b$ dataset do indeed reflect overall cooling through this era. This confirmation is especially important in light of a recent controversial suggestion that attributes the Cenozoic trend of increasing $\delta^{18}O_b$ to post-depositional alteration during burial (*14*, *15*). However, Δ_{47} temperatures are considerably warmer than previous estimates during most of the Cenozoic (Fig. 1A), with deviations of 3° to 5°C in the middle Oligocene and late Eocene and 6° to 8°C in some late Paleocene and early Eocene intervals. Our Δ_{47} data also reveal large temperature changes in the early Eocene (48 to 56 Ma) that are not apparent in the $\delta^{18}O_b$-based record.

Most of our Δ_{47} data are from the North Atlantic, a region that is seldom represented in Cenozoic climate records. The divergences from $\delta^{18}O_b$-based reconstructions could thus reflect regional differences. However, our North Atlantic $\delta^{18}O_b$ and $\delta^{13}C$ data obtained alongside the Δ_{47} measurements generally show close agreement with equivalent global records (Fig. 1, B and C, and supplementary materials). We furthermore found excellent agreement of our Δ_{47} temperatures with previous and new Δ_{47}-based temperature estimates from other locations. Our middle Miocene temperature estimates agree with results from the Indian and Southern Ocean at that time (*16*, *17*) (Fig. 1A, purple triangles). For the Eocene, North Atlantic temperatures are similar to those in the tropical and South Atlantic Ocean [Fig. 1A, yellow circle and pink stars (*18*,*19*), including the South Atlantic location that represents the backbone for the early Cenozoic global $\delta^{18}O_b$ record. Although further validation of the globally representative nature of North Atlantic temperatures awaits detailed Δ_{47} records from multiple sites, the available data point to our Δ_{47} temperatures being representative of substantial parts of the global ocean.

The consistency in Δ_{47} temperatures between different locations furthermore argues against

[1]Bjerknes Centre for Climate Research and Department of Earth Science, University of Bergen, Bergen, Norway. [2]School of Environment, Earth and Ecosystem Sciences, The Open University, Milton Keynes, UK. [3]Faculty of Geosciences, Utrecht University, Utrecht, Netherlands. [4]School of Earth and Environmental Sciences, University of St. Andrews, St. Andrews, UK. [5]Department of Earth, Planetary, and Space Science, Department of Atmospheric and Oceanic Science, Institute of the Environment and Sustainability, American Indian Studies Center, Center for Diverse Leadership in Science, University of California, Los Angeles, Los Angeles, USA. [6]Department of Earth Science, ETH Zürich, Zürich, Switzerland.
*Corresponding author. Email: nele.meckler@uib.no
†Present address: CIRES, University of Colorado, Boulder, CO, USA.

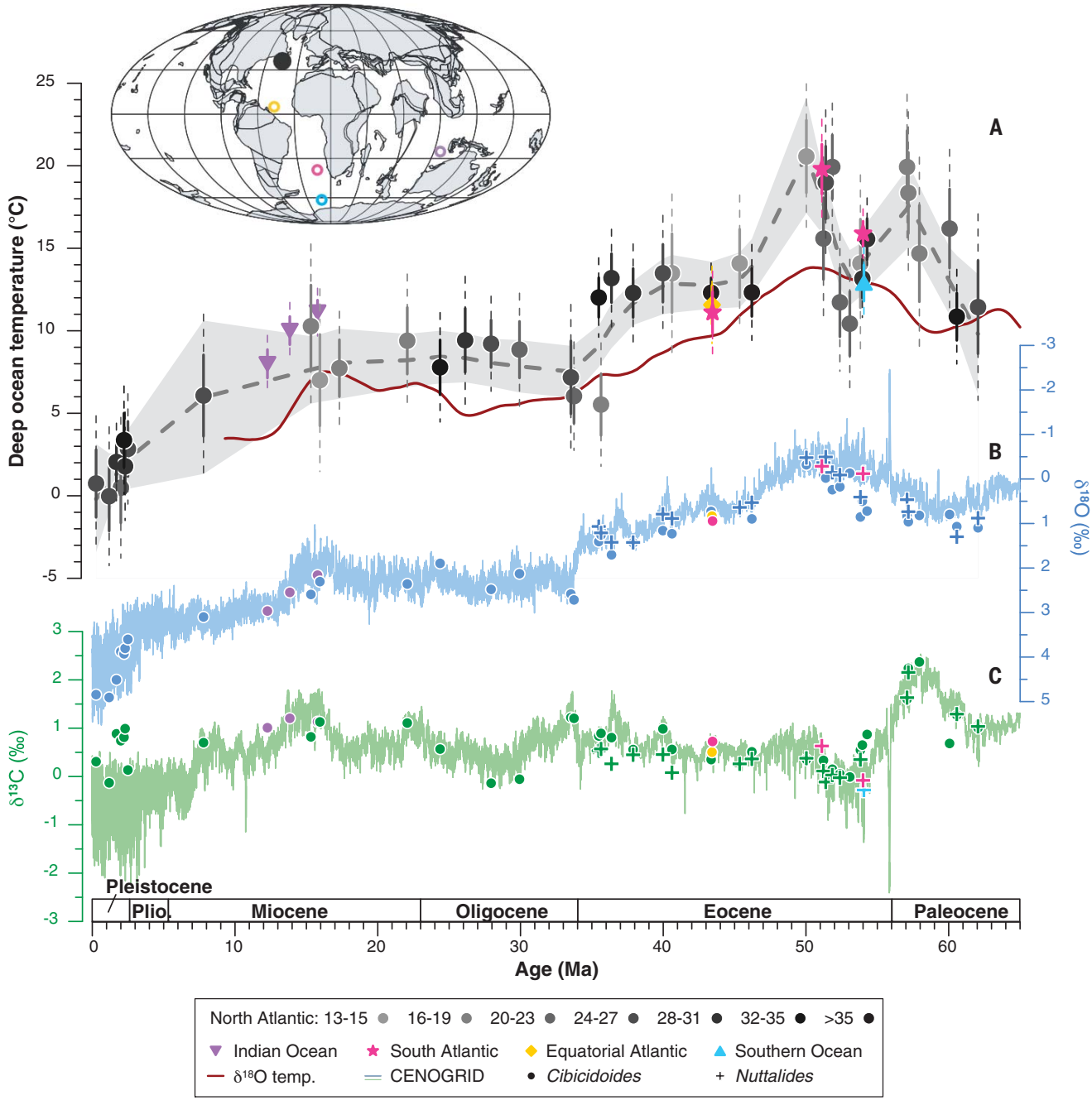

Fig. 1. Clumped isotope–based reconstruction of deep ocean temperatures compared with classical foraminifera isotope records. (**A**) Δ_{47} temperatures from the North Atlantic (gray symbols) compared with estimates from other sites (colored symbols; see inset map) in the Indian Ocean [middle Miocene (*16*)], equatorial and South Atlantic [this study (*18*, *19*)], and the Atlantic sector of the Southern Ocean (*18*). The early Eocene data from (*18*) span a time interval of ~200,000 years and were combined into one data point for each location. Error bars for Δ_{47} temperatures are 68% (solid lines) and 95% (stippled lines) confidence intervals. For the North Atlantic data, darkness of shading reflects robustness based on degree of replication, with ranges of replicate numbers specified in the figure legend. The other data points are based on 51 to >200 measurements (see data S1) reflected in the size of the error bars. The gray stippled line is a LOESS fit through the North Atlantic data with a Monte Carlo–based 95% confidence interval (see the supplementary materials), and is meant as visual guidance rather than as an alternative representation of the data. The red line is a previous estimate of deep ocean temperature based on $\delta^{18}O_b$ and sea-level reconstructions (*6*). (**B**) CENOGRID $\delta^{18}O_b$ record (*2*) and $\delta^{18}O_b$ results from species of the genus *Cibicidoides* (circles) and *Nuttalides* (crosses) from the clumped isotope analyses, corrected for interspecies offsets (*Cibicidoides:* +0.64‰; *Nuttalides:* +0.4‰). (**C**) CENOGRID $\delta^{13}C$ record (*2*) with results from *Cibicidoides* and *Nuttalides* species from the clumped isotope analyses. Note that the global CENOGRID record also includes corrections for offsets between sites and ocean basins, which we do not apply to our data. Typical offsets in $\delta^{18}O_b$ between Atlantic and Pacific sites (the latter interpreted as equivalent to global) are on the order of −0.2 to −0.3‰ for the Eocene to Oligocene (*2*), compared with 0 to −0.5‰ offsets in our *Nuttalides* data. Inset map shows site locations on a paleogeographic reconstruction for ~50 Ma (www.odsn.de/odsn/services/paleomap/paleomap.html). Also see fig. S4 for close-up views of early and late Cenozoic interval data.

a strong influence of postdepositional alteration of the Δ_{47} signal that would likely be site specific. Preservation of foraminifera at the North Atlantic sites is typically good to excellent (fig. S2), and thus is superior to many other deep ocean locations from which $\delta^{18}O$ data have been generated, and we observed no relationship between foraminifer preservation state or burial depth and Δ_{47} temperature (figs. S1 and S2). Our Pleistocene Δ_{47}-based temperatures of 0.0° to 3.4°C (fig. S4) are in agreement with observed present-day temperatures (~3°C) and reconstructed glacial temperatures [–1°C; (*20*)], further attesting to the reliability of the clumped isotope temperatures.

The deviation of Δ_{47}-based temperatures from $\delta^{18}O_b$-based temperatures could imply that deep ocean $\delta^{18}O_{sw}$ was higher than previously

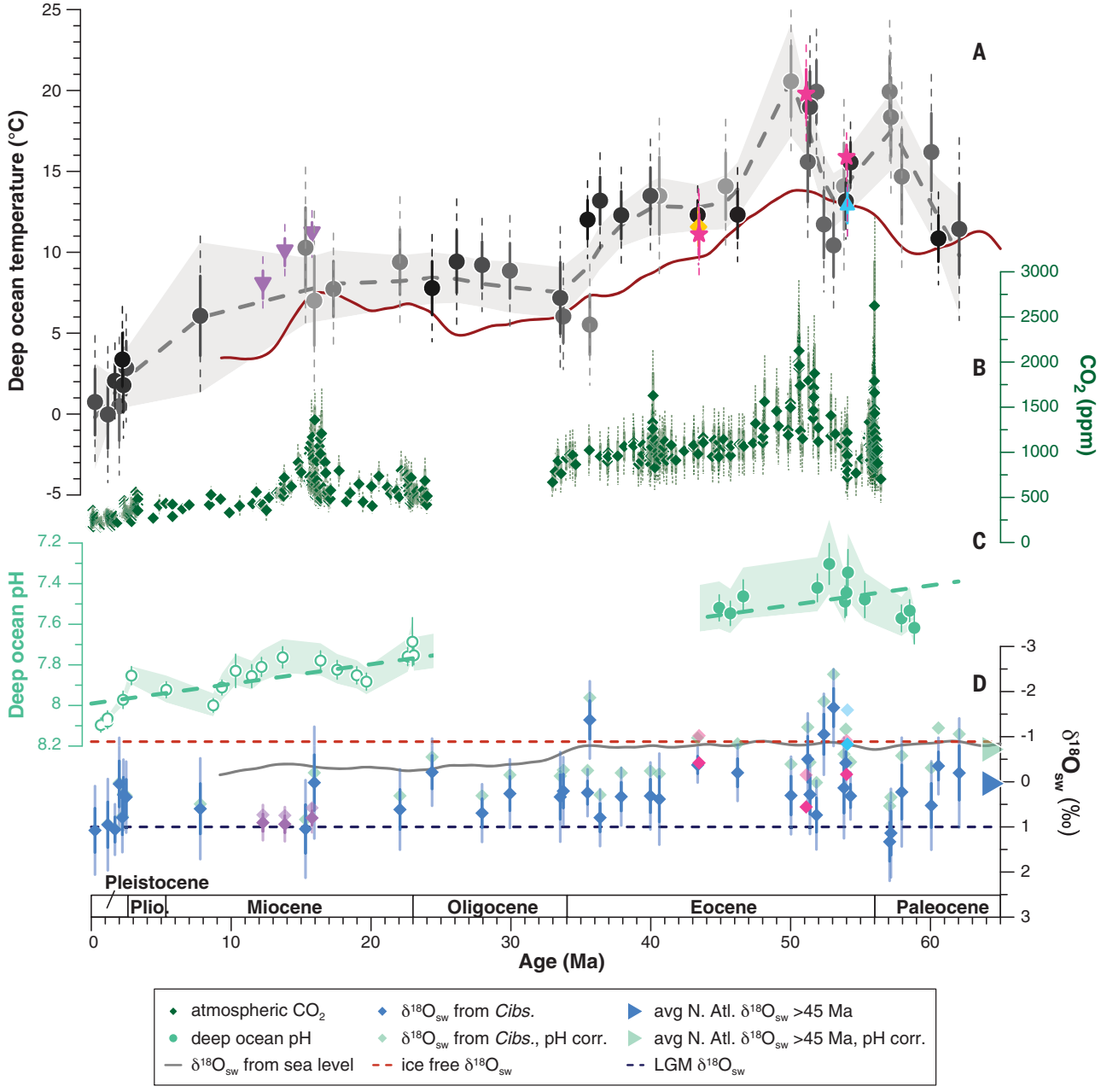

Fig. 2. Cenozoic evolution of seawater isotopic composition and comparison with changes in the carbon cycle. (**A** to **C**) Δ_{47} temperatures as in Fig. 1 (A) with atmospheric CO_2 concentration from boron isotopes in planktic foraminifera (*24*) with 1 and 2 SD (stippled lines) uncertainties (B), and reconstructed deep ocean pH from boron isotopes in benthic foraminifera [(*40*), open symbols; this study, closed symbols] with linear regression (C). Error bars show the influence of uncertainties in $\delta^{11}B$ and temperature at 2 SDs and the shaded area reflects the influence of $\delta^{11}B_{sw}$ ± 0.5‰ (see the materials and methods). (**D**) Calculated $\delta^{18}O_{sw}$ (against the SMOW standard; blue/purple symbols with 68 and 95% confidence intervals) compared with suggested "ice-free" $\delta^{18}O_{sw}$ of –0.9 ‰ [red stippled line; (6)], $\delta^{18}O_{sw}$ of Pleistocene glacial periods of 1‰ (dark blue stippled line), and $\delta^{18}O_{sw}$ reconstructed from sea-level estimates and the estimated ice-free $\delta^{18}O_{sw}$ [gray line; (6)]. Blue data points are from the North Atlantic, and other colors reflect other sites (see Fig. 1). Light green and other faded color symbols are $\delta^{18}O_{sw}$ estimates after correcting $\delta^{18}O_b$ for the long-term increase in deep ocean pH (regression line in C) and assuming a sensitivity of 1.42 ‰ per pH unit (*26*). Although this first-order correction does not eliminate the variability in $\delta^{18}O_{sw}$, it brings the values on |average in closer agreement with the estimated ice-free $\delta^{18}O_{sw}$ for the early part of the record. Arrows on the right show the average North Atlantic $\delta^{18}O_{sw}$ values for >45 Ma before (blue) and after (light green) pH correction.

thought (Fig. 2D, blue symbols versus gray line), for example, because of intensified crustal interaction with seawater due to faster seafloor spreading or from substantial continental storage of ^{16}O in ice sheets or as groundwater. Reconstructions of seafloor spreading rates show large variations but no consistent trend across the Cenozoic (*21*). $\delta^{18}O_{sw}$ values, calculated from Δ_{47} temperatures, regularly approach 1‰ in the North Atlantic and other locations [Fig. 2D (*16*)]. If wholly explained by continental ice sheets, then this would imply that ice sheets reached sizes similar to those in the Last Glacial Maximum, which seems implausible. Nevertheless, uncertainties in the size of Cenozoic ice sheets translate into uncertainties in $\delta^{18}O_{sw}$ and thus could contribute to the discrepancies in temperature estimates from Δ_{47} and $\delta^{18}O_b$. Enhanced storage of ^{16}O-enriched groundwater could also have increased $\delta^{18}O_{sw}$ and has been proposed for the Cretaceous greenhouse [e.g., (*22*)], but the magnitude of this effect is uncertain (*23*). Parts of the ocean interior could at times have been filled with more saline ^{18}O-enriched water. Overall, any of these factors or a combination of them could have contributed to elevating $\delta^{18}O_{sw}$ during much of the Cenozoic, but their potential influence remains unclear.

Instead of an underestimation of $\delta^{18}O_{sw}$, another possibility is that the incorporation of the $\delta^{18}O$ signal in foraminifera could be affected by nonthermal influences such as ocean pH. On the basis of new and published boron isotope data ($\delta^{11}B$) from benthic foraminifera, we reconstructed a pH increase of ~0.6 pH units in the deep ocean over the course of the Cenozoic (Fig. 2C), corresponding to a substantial decrease in atmospheric CO_2 concentration [Fig. 2B (*24, 25*)]. Although evidence for a pH effect on $\delta^{18}O_b$ has not yet been determined experimentally (*7*), the theoretical effect of 1.42‰ per pH unit (*26*), as observed in planktic foraminifera (*27*), would bias early Cenozoic $\delta^{18}O_b$-based temperatures by ~4°C. A pH influence on Δ_{47}, if present, would bias those temperatures in the same direction, but the effect should be approximately four times smaller than for $\delta^{18}O_b$-derived temperatures (*28*, *29*), and has so far not been observed in the typical oceanic pH range (*30*). Although we cannot conclusively demonstrate a pH effect on benthic $\delta^{18}O_b$, it is intriguing that correcting $\delta^{18}O_b$ for the overall Cenozoic trend in deep ocean pH, assuming the same effect as in planktic species (Fig. 2D, light green symbols), brings the calculated $\delta^{18}O_{sw}$ into closer agreement with previous estimates based on sea-level reconstructions (*6*): The average $\delta^{18}O_{sw}$ for >45 Ma becomes −0.72‰ versus 0.04‰ without pH correction (Fig. 2D). This improved agreement points to a pH effect being a likely explanation for the long-term disagreement between $\delta^{18}O_b$- and Δ_{47}-based temperatures. Renewed efforts should focus on investigating pH effects on $\delta^{18}O$ and Δ_{47} in benthic foraminifera to test this hypothesis.

Superimposed on the general trend in Δ_{47} temperatures, some intervals, such as the late Eocene and especially the late Paleocene to early Eocene, stand out with substantial temperature variability that is not apparent to the same extent in our $\delta^{18}O_b$ data or the global $\delta^{18}O_b$ record (Fig. 1 A and B). Although the late Eocene variability currently hinges on one anomalously cold data point at ~35.6 Ma, which could correspond to a previously reported late Eocene cooling event in the North Atlantic and elsewhere (*31*), the temperature variations in the late Paleocene to early Eocene appear to be of longer duration and are better constrained. There, we observe multi-million-year-long temperature swings with a first warming of ~4°C between 58 and 57 Ma, followed by cooling of ~4°C between 57 and 54 Ma, further ~3°C cooling between 54 and 53 Ma, and a second, major warming of 7° to 8°C at 52 Ma (Fig. 1 and fig. S4). Distinct cold spells around 55 Ma have previously been reported for the North Atlantic region (*32*), and the Δ_{47} temperatures from (*18*) show that these extended to the deep South Atlantic (Fig. 1A, pink stars and blue triangle).

The early Eocene is characterized by strong orbital-scale climate variability depicted by variations in $\delta^{18}O_b$ (*2*) of up to 1‰ (4° to 5°C using traditional assumptions), which, in principle, could have been aliased by our lower-resolution Δ_{47} sampling. However, the $\delta^{18}O_b$ data that we obtained with the Δ_{47} measurements do not show anything resembling the scale of variability suggested by Δ_{47}. This discrepancy between Δ_{47} and $\delta^{18}O_b$ is reflected in the substantial temporal variability in calculated $\delta^{18}O_{sw}$. Given the large variations in atmospheric CO_2 of up to 1000 ppm during the early Eocene [Fig. 2B (*25*)], it is likely that deep ocean pH changed more frequently and substantially over this interval than our $\delta^{11}B$ record shows. Such changes in pH could dampen any high-amplitude temperature variance recorded in $\delta^{18}O_b$. However, pH-induced dampening can likely not explain the full scale of the difference between $\delta^{18}O_b$ and Δ_{47}, because such short-lived pH changes would have to have been of similar or larger magnitude as the increase observed over the whole Cenozoic era. Changes in crustal exchange and ice volume are similarly unlikely causes for these comparatively rapid fluctuations in $\delta^{18}O_{sw}$ under peak greenhouse warmth. Instead, the early Paleogene $\delta^{18}O_{sw}$ signal is best explained by changes in deep ocean salinity, with colder temperatures between 54 and 52 Ma accompanied by fresher deep water (low $\delta^{18}O_{sw}$) and peak temperatures at 52 to 49 Ma and 57 to 60 Ma associated with high $\delta^{18}O_{sw}$ values, implying saltier deep water.

Tectonic activity and seafloor spreading in the northern North Atlantic intensified at ~57 Ma, diminished at 52 Ma, and intensified again at 48 Ma (*33*), which may have modified Arctic–North Atlantic oceanic connections, with potentially major effects on Atlantic Ocean circulation. The transitions to colder and fresher deep water sometime between 57 and 54 Ma and back to warm salty deep water at 52 Ma also roughly coincide with a marked increase and subsequent decrease in $\delta^{13}C_b$ (Fig. 1C) that may reflect changes in ocean circulation. Early Eocene changes in ocean circulation are also indicated by nitrogen and sulfur isotope records [fig. S7 (*34, 35*)], suggesting shifts from low-latitude warm, oxygen-poor intermediate, deepwater mass sources to high-latitude, colder, oxygen-rich sources. These latter biogeochemical tracers suggest stepwise changes rather than the transient temperature swings revealed by Δ_{47}, possibly because they reflect intermediate rather than deepwater masses and/or changes in other ocean basins that might differ from those in the deep Atlantic. Regardless, multiple lines of evidence indicate large-scale reorganizations in water mass structure in the Atlantic, and possibly the global ocean, during the early Paleogene.

The observed switches between warm and cold deepwater masses with inferred accompanying changes in salinity imply the need to reassess the interpretation of $\delta^{18}O_b$ records. Temperature and salinity are the key determinants of seawater density; given that both influence $\delta^{18}O_b$, $\delta^{18}O_b$ has previously been invoked as an integrated proxy for seawater density (*36*) rather than for either of the underlying parameters in isolation. Calculating density from $\delta^{18}O_b$ is, however, complicated by large variations in the relationship between $\delta^{18}O_{sw}$ and salinity (*36*). Nonetheless, at any given depth in the deep ocean, density is likely more stable than temperature or salinity alone, which could explain why $\delta^{18}O_b$ does not record the temperature swings that we observed with Δ_{47}. During the early Eocene, latitudinal temperature gradients were reduced [e.g., (*8*)], salinity gradients were enhanced because of a stronger hydrological cycle (*37*), and shallow tropical seas were more widespread. Under these conditions, saline water masses originating at low to mid latitudes could have been more prevalent at times. Density differences may have been small enough to allow for the coexistence of, and switches between, water masses of very different temperatures and/or salinities, as has been proposed for the Paleocene-Eocene Thermal Maximum [e.g., (*38*)]. On time scales shorter than possible variations in the global ocean water isotope budget, the overall isotope budget must stay balanced, calling for freshening in other parts of the ocean during times when the deep Atlantic Ocean was filled with saltier water. Our data suggest that the early Eocene greenhouse was characterized by a more dynamic deep water mass structure than was previously thought.

The strong temperature variations that we observed in the deep Atlantic during the early Eocene are not reflected in the contemporaneous sea surface temperature records available (fig. S5). Although there is a geographic scarcity of records and a potential for large geographic differences in sea surface temperatures (*39*), at face value, this discrepancy between deep ocean and sea surface temperatures lends support to changes in the structure of deep water masses being the main cause of the strong deep ocean temperature variations rather than wholesale swings in global mean temperature. However, the pronounced warming at 52 Ma coincides with a marked increase in reconstructed atmospheric CO_2 [Fig. 2B (*24, 25*)], calling for increased focus on detailed temperature reconstructions from both the surface and deep ocean across this important time interval.

Whereas our data confirm the first-order Cenozoic cooling trend in the deep ocean, they also imply that our canonical views on the relationship of $\delta^{18}O_b$ with ice volume and temperature do not hold true through the Cenozoic, implying that $\delta^{18}O_b$ should not be used as a direct temperature proxy without further constraints. If our warmer deep ocean temperatures turn out to be representative of a large fraction of the global ocean, then this would lead to a higher climate sensitivity to atmospheric CO_2 during Cenozoic greenhouse climates (*5*, *18*, *25*) compared with previous $\delta^{18}O_b$-based estimates. Our finding of major variations in deep ocean temperature during the early Eocene that are not apparent in $\delta^{18}O_b$ points to additional, non-ice volume–related changes in the oxygen isotope composition of seawater potentially in combination with changes in deep ocean pH masking the temperature effect in $\delta^{18}O_b$. Together, these constraints on deep ocean properties emerging from the application of clumped isotope thermometry offer the opportunity to investigate, not only overall greenhouse climate states, but also climate (in)stability under such warmer-than-modern boundary conditions.

REFERENCES AND NOTES

1. J. Zachos, M. Pagani, L. Sloan, E. Thomas, K. Billups, *Science* **292**, 686–693 (2001).
2. T. Westerhold *et al.*, *Science* **369**, 1383–1387 (2020).
3. D. J. Lunt *et al.*, *Clim. Past* **17**, 203–227 (2021).
4. K. D. Burke *et al.*, *Proc. Natl. Acad. Sci. U.S.A.* **115**, 13288–13293 (2018).
5. G. N. Inglis *et al.*, *Clim. Past* **16**, 1953–1968 (2020).
6. B. S. Cramer, K. G. Miller, P. J. Barrett, J. D. Wright, *J. Geophys. Res.* **116** (C12), C12023 (2011).
7. T. M. Marchitto *et al.*, *Geochim. Cosmochim. Acta* **130**, 1–11 (2014).
8. C. J. Hollis *et al.*, *Geosci. Model Dev.* **12**, 3149–3206 (2019).
9. M. E. Katz *et al.*, *Paleoceanography* **18**, 1024 (2003).
10. A. Tripati, J. Backman, H. Elderfield, P. Ferretti, *Nature* **436**, 341–346 (2005).
11. C. H. Lear, H. Elderfield, P. A. Wilson, *Science* **287**, 269–272 (2000).
12. C. H. Lear, E. M. Mawbey, Y. Rosenthal, *Paleoceanography* **25**, PA4215 (2010).
13. J. M. Eiler, *Earth Planet. Sci. Lett.* **262**, 309–327 (2007).
14. S. Bernard, D. Daval, P. Ackerer, S. Pont, A. Meibom, *Nat. Commun.* **8**, 1134 (2017).
15. D. Evans *et al.*, *Nat. Commun.* **9**, 2875 (2018).
16. S. E. Modestou, T. J. Leutert, A. Fernandez, C. H. Lear, A. N. Meckler , *Paleoceanogr. Paleoclimatol.* **35**, e2020PA003927 (2020).
17. T. J. Leutert, S. Modestou, S. M. Bernasconi, A. N. Meckler, *Clim. Past* **17**, 2255–2271 (2021).
18. T. Agterhuis, M. Ziegler, N. J. de Winter, L. J. Lourens, *Commun. Earth Environ* **3**, 39 (2022).
19. T. J. Leutert *et al.*, *Geochim. Cosmochim. Acta* **257**, 354–372 (2019).
20. N. Thiagarajan, A. V. Subhas, J. R. Southon, J. M. Eiler, J. F. Adkins, *Nature* **511**, 75–78 (2014).
21. R. D. Müller, M. Sdrolias, C. Gaina, B. Steinberger, C. Heine, *Science* **319**, 1357–1362 (2008).
22. J. E. Wendler, I. Wendler, C. Vogt, J. Kuss, *Palaeogeogr. Palaeoclimatol. Palaeoecol.* **441**, 430–437 (2016).
23. A. Davies *et al.*, *Cretac. Res.* **112**, 104445 (2020).
24. J. W. B. Rae *et al.*, *Annu. Rev. Earth Planet. Sci.* **49**, 609–641 (2021).
25. E. Anagnostou *et al.*, *Nat. Commun.* **11**, 4436 (2020).
26. R. E. Zeebe, *Palaeogeogr. Palaeoclimatol. Palaeoecol.* **170**, 49–57 (2001).
27. H. J. Spero, J. Bijma, D. W. Lea, B. E. Bemis, *Nature* **390**, 497–500 (1997).
28. A. K. Tripati *et al.*, *Geochim. Cosmochim. Acta* **166**, 344–371 (2015).
29. W. F. Guo, *Geochim. Cosmochim. Acta* **268**, 230–257 (2020).
30. J. W. Tang, M. Dietzel, A. Fernandez, A. K. Tripati, B. E. Rosenheim, *Geochim. Cosmochim. Acta* **134**, 120–136 (2014).
31. K. K. Śliwińska, E. Thomsen, S. Schouten, P. L. Schoon, C. Heilmann-Clausen, *Sci. Rep.* **9**, 4458 (2019).
32. M. L. Vickers *et al.*, *Nat. Commun.* **11**, 4713 (2020).
33. C. Gaina, J. Jakob, *Tectonophysics* **760**, 136–151 (2019).
34. V. C. F. Rennie *et al.*, *Nat. Geosci.* **11**, 761–765 (2018).
35. E. R. Kast *et al.*, *Science* **364**, 386–389 (2019).
36. J. Lynch-Stieglitz, W. B. Curry, N. Slowey, *Paleoceanography* **14**, 360–373 (1999).
37. J. Zhu *et al.*, *Earth Planet. Sci. Lett.* **537**, 116164 (2020).
38. A. Tripati, H. Elderfield, *Science* **308**, 1894–1898 (2005).
39. P. M. J. Douglas *et al.*, *Proc. Natl. Acad. Sci. U.S.A.* **111**, 6582–6587 (2014).
40. R. Greenop *et al.*, *Clim. Past* **13**, 149–170 (2017).
41. A. N. Meckler *et al.*, Cenozoic clumped isotope temperature record from the deep North Atlantic for: Cenozoic evolution of deep ocean temperature from clumped isotope thermometry, Version 1.0, EarthChem (2022); https://doi.org/10.26022/IEDA/112213.
42. A. N. Meckler *et al.*, Clumped isotope deep-sea temperature data in the South Atlantic for the Early Eocene Climatic Optimum from Meckler *et al.* (2022) for: Cenozoic evolution of deep ocean temperature from clumped isotope thermometry, Version 1.0, EarthChem (2022); https://doi.org/10.26022/IEDA/112215.
43. A. N. Meckler *et al.*, Cenozoic clumped isotope temperature record from the deep North Atlantic for: Cenozoic evolution of deep ocean temperature from clumped isotope thermometry, Pangaea (2022); https://doi.org/10.1594/PANGAEA.945578.

ACKNOWLEDGMENTS

We thank N. Irvali, R. Tapia, L. Griem, J. Donn Holl, L. Al-Saadi, V. Taylor, E. Alagoz, and E. Vinje Galaasen for technical help during sample preparation and clumped isotope analyses in Bergen; A. Fernandez Bremer for sharing Matlab code for error propagation; I. J. Kocken for processing the Utrecht clumped isotope data archive with his R script; A. Roozendaal for sample preparation in Utrecht; A. E. van Dijk for technical support in the Utrecht lab; and M. Kaminski and E. Littley for assistance with boron isotope analyses. This research used samples and data from the International Ocean Discovery Program (IODP) and the Ocean Drilling Program (ODP). The manuscript benefited from the constructive comments of the reviewers. **Funding:** This work was supported by the Swiss National Science Foundation (MHV fellowship to A.N.M.); the European Research Council (starting grant 638467 to A.N.M. and starting grant 805246 to J.W.B.R.); the Trond Mohn Foundation (starting grant BFS2015REK01 to A.N.M.); the Norwegian Research Council (infrastructure grant 245907 to A.N.M.); the Natural Environment Research Council (NERC grant NE/P019331/1 to P.F.S.); the Dutch Research Council (NWO VIDI project 016.161.365 to M.Z.); the Heising Simons Foundation (grant 2022-3314 to A.T.); and the Netherlands Earth System Science Centre (NESSC) (L.J.L.).
Author contributions: Conceptualization: A.N.M., P.F.S., A.T., M.Z., S.M.B.; Funding acquisition: A.N.M., P.F.S., M.Z., L.J.L., J.W.B.R., A.T., S.M.B.; Initiation: A.N.M., A.T.; Investigation: A.N.M., P.F.S., A.M.P., T.J.L., J.M., T.A., M.Z., L.J.L., J.B., J.W.B.R.; Methodology: A.N.M., M.Z., S.M.B.; Resources: P.F.S., J.W.B.R., L.J.L.; Writing – original draft: A.N.M., P.F.S., M.Z., J.W.B.R.; Writing – review & editing: A.N.M., P.F.S., T.J.L., J.M., M.Z., T.A., L.J.L., J.W.B.R., J.B., A.T., S.M.B.
Competing interests: The authors declare no competing interests.
Data and materials availability: Replicate-level Δ_{47} data with standard data and detailed data-processing information are available from the EarthChem database (*41*, *42*). Sample-average Δ_{47} temperatures, $\delta^{18}O_b$, and $\delta^{18}O_{sw}$ data are available in the Pangaea database (*43*) and are available in the supplementary materials as data S1. The boron isotope data from benthic foraminifera are available in the supplementary materials as data S3 and will be uploaded to the EarthChem and Pangaea databases.

SUPPLEMENTARY MATERIALS

science.org/doi/10.1126/science.abk0604
Materials and Methods
Figs. S1 to S7
Tables S1 and S2
References (*44*–*79*)
Data S1 to S3

Submitted 18 June 2021; accepted 26 May 2022
10.1126/science.abk0604

Cenozoic evolution of deep ocean temperature from clumped isotope thermometry

A. N. MecklerP. F. SextonA. M. PiaseckiT. J. LeutertJ. MarquardtM. ZieglerT. AgterhuisL. J. LourensJ. W. B. RaeJ. BarnetA. TripatiS. M. Bernasconi

Science, 377 (6601), • DOI: 10.1126/science.abk0604

Warmer than realized

Past climates may hold important clues about how the planet might respond to ongoing climate warming. Meckler *et al*. use clumped isotope thermometry on benthic foraminifera to reinterpret the record of the deep ocean temperature over the past 65 million years. They found that deep ocean temperatures were generally higher and more variable than earlier work suggests. Their results have implications for our understanding of deep sea temperature responses to atmospheric carbon dioxide concentrations, climate sensitivity, and ocean structure during times of minimal continental ice. —HJS